Journal of Dental Research
2017, Vol. 96(10) 1122–1128

DOI: 10.1177/0022034517709738
journals.sagepub.com/home/jdr

Formation of Fluorohydroxyapatite with Silver Diamine Fluoride

M.L. Mei[1], F. Nudelman[2], B. Marzec[2], J.M. Walker[2], E.C.M. Lo[1], A.W. Walls[3], and C.H. Chu[1]

Abstract

Silver diamine fluoride (SDF) is found to promote remineralization and harden the carious lesion. Hydroxyapatite crystallization is a crucial process in remineralization; however, the role of SDF in crystal formation is unknown. We designed an in vitro experiment with calcium phosphate with different SDF concentrations (0.38, 1.52, 2.66, 3.80 mg/mL) to investigate the effect of this additive on the nucleation and growth of apatite crystals. Two control groups were also prepared—calcium phosphate ($CaCl_2 \cdot 2H_2O + K_2HPO_4$ in buffer solution) and SDF ($Ag[NH_3]_2F$ in buffer solution). After incubation at 37 °C for 24 h, the shape and organization of the crystals were examined by bright-field transmission electron microscopy and electron diffraction. Unit cell parameters of the obtained crystals were determined with powder X-ray diffraction. The vibrational and rotational modes of phosphate groups were analyzed with Raman microscopy. The transmission electron microscopy and selected-area electron diffraction confirmed that all solids precipitated within the SDF groups were crystalline and that there was a positive correlation between the increased percentage of crystal size and the concentration of SDF. The powder X-ray diffraction patterns indicated that fluorohydroxyapatite and silver chloride were formed in all the SDF groups. Compared with calcium phosphate control, a contraction of the unit cell in the *a*-direction but not the *c*-direction in SDF groups was revealed, which suggested that small localized fluoride anions substituted the hydroxyl anions in hydroxyapatite crystals. This was further evidenced by the Raman spectra, which displayed up-field shift of the phosphate band in all the SDF groups and confirmed that the chemical environment of the phosphate functionalities indeed changed. The results suggested that SDF reacted with calcium and phosphate ions and produced fluorohydroxyapatite. This preferential precipitation of fluorohydroxyapatite with reduced solubility could be one of the main factors for arrest of caries lesions treated with SDF.

Keywords: calcium, phosphates, hydroxylapatite, fluor-hydroxylapatite, tooth remineralization, dental caries

Background

Silver diamine fluoride (SDF) is a topical fluoride solution that has been used for caries management. Unlike other fluoride products that prevent the formation of new caries, SDF is capable of efficiently halting the caries process (Gao et al. 2016). Recently, this caries-arresting property of SDF has drawn much attention from dental clinicians and researchers. SDF has shown its clinical success on arresting the coronal caries of the primary teeth of children (Chu et al. 2002), permanent teeth in teenagers (Chu et al. 2014), and root caries of the elderly (Tan et al. 2010). An in vitro study found that SDF increases the mineral density of the artificial carious lesion (Mei, Ito, et al. 2013); ex vivo studies investigated the collected exfoliated primary teeth from the SDF clinical trials and found that a hardened and highly mineralized zone was formed in the outermost 150 μm of an SDF-treated carious lesion (Chu and Lo 2008; Mei, Ito, Cao, Lo, et al. 2014). Silver has a well-known antibacterial effect, and previous studies demonstrated that SDF inhibited cariogenic biofilm formation (Chu et al. 2012; Mei, Chu, et al. 2013; Mei, Li, et al. 2013).

However, only a few publications report the mode of action of SDF on mineralized tissue. Yamaga et al. (1972) suggested that the formation of calcium fluoride (CaF_2) and silver phosphate could be responsible for the prevention of dental caries and the hardening of a carious lesion. However, Suzuki et al. (1974) demonstrated the formation of CaF_2 by mixing enamel powder with an SDF solution, but the amount of CaF_2 dropped significantly when the materials were immersed into artificial saliva. They also found that silver phosphate disappeared after being immersed in artificial saliva and was replaced by silver chloride (AgCl) and silver thiocyanate. In addition, Lou et al. (2011) found that a CaF_2-like material and metallic silver were formed by mixing SDF with hydroxyapatite powder and gelatine (as a chemically representative protein),

[1]Faculty of Dentistry, The University of Hong Kong, Hong Kong SAR, China
[2]EaStCHEM, School of Chemistry, The University of Edinburgh, Edinburgh, UK
[3]Edinburgh Dental Institute, The University of Edinburgh, Edinburgh, UK

Corresponding Authors:
C.H. Chu, Faculty of Dentistry, The University of Hong Kong, 34 Hospital Road, Hong Kong SAR, China.
Email: chchu@hku.hk
A.W. Walls, Edinburgh Dental Institute, Lauriston Building (Fourth Floor), Lauriston Place, Edinburgh EH3 9HA, UK.
Email: angus.walls@ed.ac.uk

but the CaF_2-like material dissolved and disappeared after washing with water. Therefore, the mode of SDF action is still unclear.

The high concentration of calcium and phosphate in saliva is the major mineral source in the oral environment. The contribution of calcium, phosphate, and hydroxyl ions present in saliva to apatite deposition is fundamental. However, to the best of our knowledge, there has been no study to investigate the role of SDF as an additive in synthetic apatite crystallization experiments. It is therefore worthwhile to study mineral structures formed in the presence of SDF to gain insights into these complex reactions (Beniash et al. 2005). Thus, this study aimed to observe the effect of SDF on hydroxyapatite crystallization occurring in vitro, whereby the observed apatite deposition was described with a simplified chemical model. The null hypothesis was that SDF had no effect on crystal formation.

Materials and Methods

Mineralization Reaction

The reaction was performed in a Tris-buffered saline (TBS) consisting of a 50mM Trizma base and 150mM sodium chloride (NaCl) in Milli-Q water set at pH 7.40. Apatite precipitation was achieved by incubating $CaCl_2$ (5.88mM; Merck Ltd.) with K_2HPO_4 (4.12mM; Merck Ltd.) in TBS at 37 °C for 24 h, as described (Habraken et al. 2013), in the presence or absence of different concentrations of SDF: 0.38 mg/mL (fluoride concentration: 45 ppm), 1.52 mg/mL (180 ppm), 2.66 mg/mL (314 ppm) and 3.80 mg/mL (448 ppm). These 4 groups containing SDF were called SDF groups. The calcium phosphate control contained $CaCl_2$ + K_2HPO_4 but no SDF. The SDF control comprised 0.38 mg/mL SDF in the TBS without $CaCl_2 \cdot 2H_2O$ + K_2HPO_4. The final pH values of each reaction were measured with a pH electrode. Samples were then analyzed with transmission electron microscopy (TEM) with energy-dispersive X-ray spectroscopy (EDS), powder X-ray diffraction (P-XRD), and Raman spectroscopy (detailed later). The experiment was done in triplicate.

Transmission and Scanning Electron Microscopy Analysis

For TEM and EDS analysis, formvar/carbon-coated 200-mesh Ni TEM grids (Agar Scientific) were plasma treated for 40 s with a Quorum sputter coater prior to use. The grids were floated upside down over a 2-mL reaction solution in a 24-well plate. At the end of the reaction, the grids were rinsed with Milli-Q water, blotted against filter paper, air-dried, and analyzed by TEM. TEM analysis was performed with a Technai F20 (FEI) equipped with a field emission gun and an Tietz CCD camera (8 × 8 k; Beniash et al. 2005). Ten crystal units were selected randomly from the TEM images, and the width and length of the crystal unit were measured with the image analysis software ImageJ (National Institutes of Health). The changes in proportions of the crystals for each group were calculated per the difference between the means of each group divided by that of the calcium phosphate control group. Selected-area electron diffraction was performed to determine the crystallographic parameters of the investigated samples. EDS was used to characterize the chemical composition of the precipitates and quantify the fluoride/calcium and fluoride/phosphorus ratios by dividing the mean atomic percentage of fluoride by either that of the calcium or that of the phosphorus.

Powder X-ray Diffraction

The reaction solution was centrifuged at 5,000 *g*, and the pellet was collected and washed thoroughly by Milli-Q water and resuspended into ethanol. A drop (~10 μL) of this suspension was deposited on a low-background Si-substrate, and the solvent was allowed to evaporate. The samples were then analyzed with a Bruker D2 Phaser P-XRD diffractometer equipped with a CuKα lamp (λ = 1.54056 Å). Data collection parameters included the following: 2θ range = 20° to 60°, step size = 0.02°, and scan speed = 0.5 s/step. Hexagonal unit cell parameters *a* and *c* were calculated according to Bragg's equation, from the (300) and (002) reflections observed in the recorded P-XRD patterns (Liu et al. 2013):

$$d = \frac{n\lambda}{2\sin\theta},$$

where *d* is the distance between symmetry-equivalent diffraction planes, *n* is the consecutive natural number, λ is the wavelength, and θ is the incident angle of the X-ray beam.

Raman Spectroscopy

Raman spectra of the samples were recorded with a Renishaw InVia Raman microscope system (3 accumulations; range, 900 to 1,500 cm^{-1}) equipped with a 785-nm laser. The laser spot size was approximately 3 μm and focused on the growth electrode, and the power was kept <1 $mW/\mu m^2$. All spectra were recorded at ambient temperature (Chen et al. 2015).

Statistical Analysis

The length and width of the crystal were assessed for a normal distribution via the Shapiro-Wilk test for normality. One-way analysis of variance with Bonferroni post hoc tests was used to detect differences between groups. Analyses were performed with the computer software SPSS 19.0 (IBM Corporation). The level of statistical significance was set at 0.05.

Results

The TEM images revealed the morphology of experimental groups and corresponding SEAD and EDS results. Apatite crystals that formed in the absence of SDF exhibited the characteristic plate-shape morphology (Kokubo et al. 2003), and selected-area electron diffraction showed the typical reflections corresponding to the (211), (002), and (112) planes of apatite.

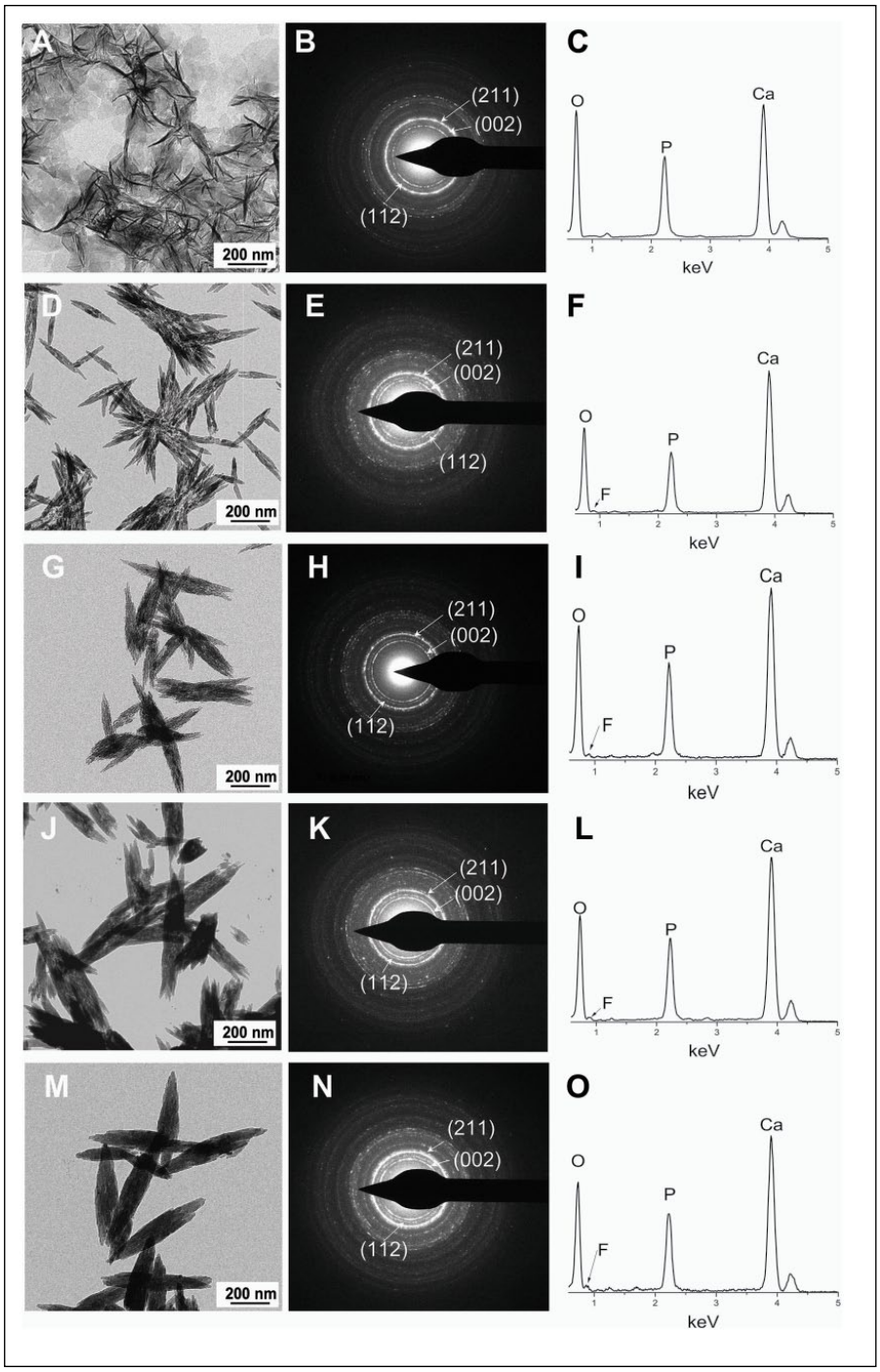

Figure 1. Transmission electron microscopy data of experimental groups. Calcium phosphate control group: (**A**) morphology, (**B**) SAED pattern, (**C**) EDS spectra. SDF group, 0.38 mg/mL: (**D**) morphology, (**E**) SAED pattern, (**F**) EDS spectra. SDF group, 1.52 mg/mL: (**G**) morphology, (**H**) SAED pattern, (**I**) EDS spectra. SDF group, 2.66 mg/mL: (**J**) morphology, (**K**) SAED pattern, (**L**) EDS spectra. SDF group, 3.80 mg/mL: (**M**) morphology, (**N**) SAED pattern, (**O**) EDS spectra. No crystal was detected in the SDF control group (no calcium phosphate). Ca, calcium; EDS, energy-dispersive X-ray spectroscopy; F, fluoride; O, oxygen; P, phosphorus; SAED, selected-area electron diffraction; SDF, silver diamine fluoride.

EDS confirmed the presence of Ca and P (Fig. 1A–C). The addition of increasing concentrations of SDF to the reaction resulted in a change in the morphology of the crystals, shifting from plate-shaped crystals (no SDF) to round-ended prismatic morphology (Fig. 1D–O). Selected-area electron diffraction showed the reflections corresponding to the (002), (211), and (112) planes, confirming that these crystals were made of apatite. Furthermore, the recorded EDS spectra contained a signal attributed to fluoride, in addition to Ca and P, confirming that fluoride was present in the investigated apatite samples. Interestingly, as the concentration of SDF increased, the crystals became longer and thicker. The width of the crystals (mean ± SD) were 14 ± 4 nm ①, 33 ± 3 nm ②, 79 ± 14 nm ③, 117 ± 17 nm ④ and 126 ± 6 nm ⑤ in the following groups, respectively: calcium phosphate control (no SDF), 0.38 mg/mL (SDF), 1.52 mg/mL, 2.66 mg/mL, and 3.80 mg/mL (①<②<③<④, ⑤; $P < 0.001$). The length of the crystals (mean ± SD) were 137 ± 25 nm ①, 273 ± 72 nm ②, 497 ± 55 nm ③, 547 ± 94 nm ④ and 650 ± 49 nm ⑤ in the following groups, respectively: calcium phosphate control (no SDF), 0.38 mg/mL (SDF), 1.52 mg/mL, 2.66 mg/mL, and 3.80 mg/mL ①<②<③, ④<⑤; $P < 0.001$). Their aspect ratios (width divided by the length) also changed, going from 0.10 to 0.19. There was a positive correlation between the increased percentage of crystal size and the concentration of SDF (Fig. 2). The increase in the width was much larger than that of the length, as reflected in the change in the aspect ratio found in Figure 2A ($m = 2.20$) to that found in Figure 2B ($m = 0.91$). As expected, no hydroxyapatite crystal was detected in the SDF control (no calcium phosphate) group.

There was a steady increase of fluoride/calcium and fluoride/phosphorus ratios in the crystal when SDF concentration went up (Table). The reaction conditions were alkaline in all the SDF groups, and the pH values increased when SDF concentrations increased. The pH value measured in the group containing calcium phosphate was 7.07; this drop of pH from the original 7.40 suggested that a hydroxyl ion was incorporated into crystal and that more hydrogen ions were

Table. Calculated Hexagonal Unit Cell Parameters *a* and *c* Axes, F/Ca, F/P, and Final pH in Experimental Groups.

	P-XRD, Å				
SDF,[a] mg/mL	*a*-axis	*c*-axis	F/Ca	F/P	Final pH
None[b]	9.577 ± 0.0012	6.833 ± 0.0010	N/A	N/A	7.07 ± 0.02
0.38	9.554 ± 0.0011	6.833 ± 0.0010	0.022 ± 0.002	0.043 ± 0.006	8.02 ± 0.01
1.52	9.552 ± 0.0036	6.833 ± 0.0010	0.037 ± 0.007	0.055 ± 0.006	8.14 ± 0.01
2.66	9.548 ± 0.0024	6.833 ± 0.0010	0.043 ± 0.004	0.070 ± 0.009	8.60 ± 0.02
3.80	9.542 ± 0.0047	6.833 ± 0.0010	0.072 ± 0.005	0.111 ± 0.011	8.95 ± 0.01

All the data are normally distributed. Values are presented as mean ± SD.
F/Ca, fluoride/calcium; F/P, fluoride/phosphorus; N/A, not applicable; P-XRD, powder X-ray diffraction; SDF, silver diamine fluoride.
[a]No crystal was detected in the SDF control group (no calcium phosphate).
[b]Calcium phosphate control.

released (Habraken et al. 2013). All the results indicate the formation of fluorohydroxyapatite in all of the SDF groups, whereby the fluoride content increased with SDF concentration.

The typical P-XRD pattern of the experimental groups is shown in Figure 3A. The P-XRD analysis indicated that the solids precipitated in the calcium phosphate control group scattered X-rays similarly to hydroxyapatite. However, the reflections were sharper in SDF groups than in the calcium phosphate control group—in particular, the hydroxyapatite (211) and (300) reflections. The (300) reflections in SDF groups were shifted slightly from ~32.3° (2θ) to ~33.2° (2θ) as compared with the calcium phosphate control group (Fig. 3B). The (002) reflection was not significantly changed. This pattern of reflection is similar to the one of fluorohydroxyapatite previously reported (Chen and Miao 2005). These shifts also reflect the contraction of the calculated unit cell parameters, as summarized in the Table. Apart from apatite, the strong reflections at 27.88°, 32.28°, and 46.28° in the SDF groups and the SDF control group (no calcium phosphate) were coincident with AgCl (111), (200), and (220) reflections, which suggested that AgCl precipitated as a separate phase in the SDF-containing samples. Traces of silver oxide were also detected in the 0.38-mg/mL SDF group.

The Raman spectra showed that all experimental groups displayed a strong PO_4^{3-} band at ~960 cm^{-1}, except for the SDF control group (no calcium phosphate; Fig. 4). The PO_4^{3-} band associated with the P-O stretch shifted from 961 cm^{-1} in the calcium phosphate control group (no SDF) to ~965 cm^{-1} in SDF groups, indicating a change of the phosphate group environment and suggesting—based on the composition of the reaction mixture—a substitution of the hydroxyl groups with more electronegative fluoride anions.

Discussion

This study was the first to investigate the effect of SDF on remineralization progress in the context of crystal formation. The null hypothesis was rejected according to the results of this research. SDF clearly altered the crystal structure of the precipitated minerals, and its presence enabled the formation of fluorohydroxyapatite. This observation helps to build the understanding of the role of SDF in the remineralization of caries.

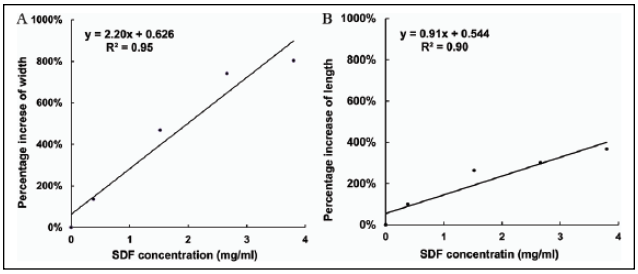

Figure 2. Pearson correlation between the percentage increase of crystal size and SDF concentrations. (**A**) The correlation between percentage increase of width of crystal and SDF concentration (coefficient R^2 = 0.95, slope m = 2.20). (**B**) The correlation between percentage increase of length of crystal and SDF concentration (coefficient R^2 = 0.90, slope m = 0.91). SDF, silver diamine fluoride.

In this study, we adopted a buffered calcium phosphate system to perform the reaction; this system has been shown to be able to start an initial deposition of amorphous calcium phosphate, and it favors subsequent transformation into small crystals of apatite and ultimate growth of ripening of those crystals (Termine and Posner 1970). However, this might be different from the real situation. Another limitation of the chemical system is the lack of biological component, in which the role of silver could be underestimated. This chemical system is very different from complex in vivo situation; thus, caution should be exercised in data interpretation.

Although the commercial SDF solution (Saforide) has a high concentration of silver (255,000 ppm) and fluoride (448,000 ppm), clinical treatment will consist of a onetime application of a minute volume of the solution (0.22 ± 0.07 mg) to carious lesions (Chu et al. 2012). In the clinical setting, the SDF will be readily diluted by saliva in the oral cavity. The volume of saliva in the mouth is around 0.60 mL (Lagerlöf and Dawes 1984). The concentration of SDF per application is approximately 0.22/0.60, or 0.36 mg/mL. Given this assumption, we arbitrarily selected several concentrations from 0.38 to 3.80 mg/mL in this study.

Saliva plays a crucial role in the caries remineralization progress. It is a buffered system, supersaturated with respect to calcium phosphate, whereby proline- and tyrosine-rich proteins inhibit the excessive nucleation of apatite phases (Schwartz et al. 1992). The salivary activities of calcium and phosphate ions

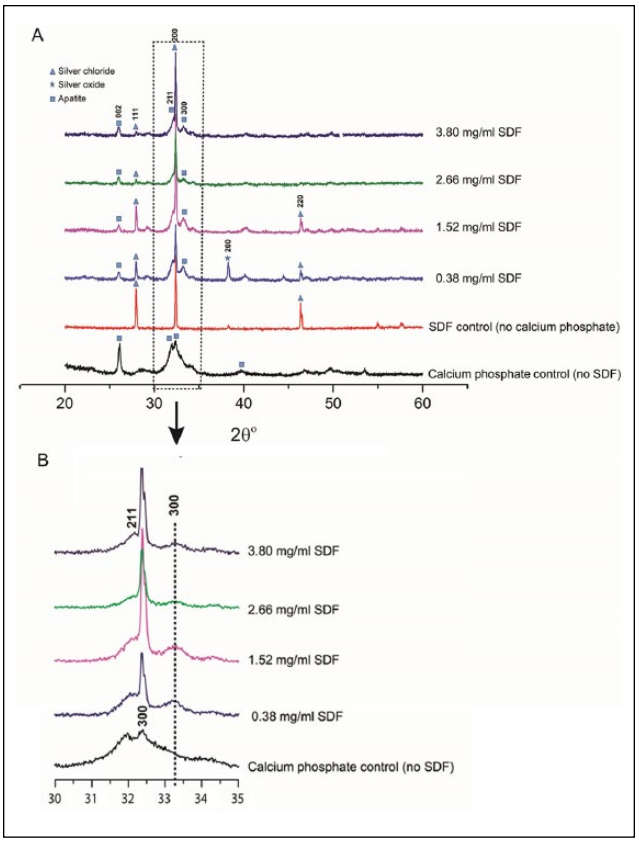

Figure 3. Typical powder X-ray diffraction patterns of the experimental groups: (**A**) range, 20° to 60°; (**B**) range, 30 to 35°. SDF, silver diamine fluoride.

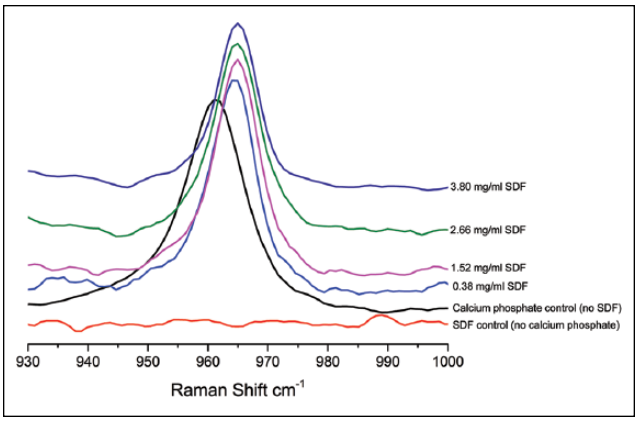

Figure 4. Raman vibrational spectra of the experimental groups: range, 930 to 1,000 cm^{-1}. SDF, silver diamine fluoride.

are important because both species are part of the hydroxyapatite unit cell. Therefore, saliva offers a protective and reparative environment for teeth. The calcium and phosphate ions provided by $CaCl_2$ + K_2HPO_4 in TBS were a basic simulation of this salivary environment. TEM grids were explicitly floated upside down during the incubation to prevent the sedimentation of particles formed by homogeneous nucleation on their surfaces (Majewski and Allidi 2006). In this study, we demonstrated that SDF reacted with calcium and phosphate from the salivary environment and formed fluorohydroxyapatite. Apart from the salivary environment, the residual mineral crystals of the tooth could be another important factor of remineralization; the crystals serve as nucleation site for the newly formed fluorohydroxyapaptite to precipitate (Peters et al. 2010), or they promote the ion exchange of F^- for OH^- (Ogard et al. 1994). However, the exchange of the F^- for OH^- requires an acidic microenvironment to dissolve the tooth mineral to release OH^-. SDF is very alkaline (pH ~10). This alkaline property matches the favorable condition to synthesize fluorohydroxyapatite in chemistry (Chen and Miao 2005), which may hasten the reaction process by promoting precipitation.

The hydrogen ions (H^+) of the hydroxyapatite were arranged in the atomic interstices neighboring the oxygen ions (O^{2-}). The OH^- conferred a certain degree of disorder to the crystal structure of hydroxyapatite (Chen and Miao 2005). An increase in the vibrational frequency of phosphate in the SDF groups was observed in Raman spectra, which indicates the substitution of OH^- with more electronegative F^- (Chen et al. 2015). The isotropic distribution of charge on F^- anions allows for a better fit in the lattice as compared with the larger asymmetric OH^- ion (Robinson et al. 2004), thus reducing lattice microstrain and enabling fluorohydroxyapatite crystals to form larger particles. This alternating arrangement produces a fairly well-ordered apatite structure, which is characterized with increased thermal and chemical stability when compared with hydroxyapatite (Chen and Miao 2005). In addition, since F^- is smaller than OH^-, the substitution results in a noticeable contraction in the *a*-axis dimensions of the lattice (Table; Wei et al. 2003; Liu et al. 2013).

The P-XRD pattern showed that the calcium phosphate control group diffracted poorly (Fig. 3). It is plausible that the unit cell of calcium phosphate was large and flexible enough to accommodate other matters. This reduced the X-ray coherence length and resulted in broader reflections with Low intensities. P-XRD relies on Bragg's law. There is no scattering when there is no *d*-spacing. In addition, the Ca/P ratio was 1.95 in the 0.38-mg/mL SDF group. However, for the SDF concentrations ≥1.52 mg/mL, the ratios varied between 1.48 and 1.62, which was consistent with apatite minerals. Furthermore, EDS provided a semiquantitative view of the elemental composition in the inspection field in units of weight/atomic percentage. It might not be suitable to determine the precise stoichiometric determination of the ratios between calcium and phosphate in the samples.

We detected enlarged apatite crystal sizes in the SDF groups, and the size of the crystals increased with the increase in SDF concentration. This is consistent with a previous bone study, which showed that fluoride uptake is accompanied by an increase in the apatite crystal size (Eanes and Hailer 1998). It is plausible that the introduction of well-localized, isotropic, negatively charged F^- increases the stability of the structure and reduces the amount of defects related to the lattice strain. Therefore, single-crystalline domains may grow larger before their growth is interrupted by a crack or irreparable dislocation. We also found that this increase of crystal size took place

predominantly in its width but not in its length (Fig. 2). Fluoride stabilized preferentially the lateral growth against aberrant outgrowths, thus promoting a more orderly growth of new accretion layers (Eanes and Hailer 1998). The collagen matrix plays an important organizational role in establishing the manner of the crystal arrangements as well as placing some spatial constraints on their size and shape (Eanes and Hailer 1998). Further studies can be performed to address this aspect.

We did not find CaF_2, probably because of the low concentration of SDF used in this study. Other studies found that CaF_2 was not stable (Suzuki et al. 1974; Lou et al. 2011). The amount of CaF_2 significantly dropped after being immersed into artificial saliva (Suzuki et al. 1974) or disappeared after being washed with water (Lou et al. 2011). Although immersion into artificial saliva or washing with water was to mimic the salivary fluid in a clinical situation, this way of rinsing samples after exposure to SDF was susceptible to remove surface precipitation. Ogard et al. (1994) showed that CaF_2 serves as a source of fluoride for the formation of fluorapatite. However, other investigators questioned the formation of CaF_2 within clinically relevant exposure times from concentrated fluoride solutions (Bruun and Givskov 1993; Attin et al. 1995). Attin et al. (1995) showed that 80% of the CaF_2 was lost in 5 d after fluoride varnish application. Bruun and Givskov (1993) reported that CaF_2 (or its likes) was not formed in measurable amounts on sound tooth. It is generally agreed that a fluoride-releasing reservoir system is effective at low pH (Ogard et al. 1994; ten Cate 1997). SDF is alkaline. Its mechanism can be different from other acidic fluoride products. We found that SDF played a role in crystallization and induced the formation of fluorohydroxyapatite. The signature of silver was not detected in the TEM/EDS experiment, which confirms that silver ions do not occlude within the newly formed fluorohydroxyapatite lattice. The only species originating from SDF that clearly had an effect on fluorohydroxyapatite precipitation were the fluoride anions that substituted the hydroxyl ions in the crystal.

Apart from calcium phosphate, AgCl is a principal silver product that was detected with P-XRD. This result is consistent with previous studies (Suzuki et al. 1974; Mei, Ito, et al. 2013). AgCl has a low solubility (8.9×10^{-5} g/100 mL), which might also contribute to the increased hardness of a carious lesion. Nevertheless, it has been shown that a silver ion has an antibacterial effect against cariogenic bacteria (Chu et al. 2012; Mei, Chu, et al. 2013; Mei, Li, et al. 2013) and inhibits the collagenases degrading of dentine collagen (Mei et al. 2012; Mei, Ito, Cao, Li, et al. 2014).

In summary, the present study demonstrated that SDF reacts with calcium and phosphate ions and produces fluorohydroxyapatite. This preferential precipitation of fluorohydroxyapatite with reduced solubility could be one of the main factors for arrest of caries lesions treated with SDF.

Author Contributions

M.L. Mei, contributed to conception, design, data acquisition, analysis, and interpretation, drafted and critically revised the manuscript; F. Nudelman, A.W. Walls, C.H. Chu, contributed to conception, design, and data interpretation, critically revised the manuscript; B. Marzec, J.M. Walker, contributed to data interpretation, critically revised the manuscript; E.C.M. Lo, contributed to conception, critically revised the manuscript. All authors gave final approval and agree to be accountable for all aspects of the work.

Acknowledgments

This study was supported by Hong Kong–Scotland Partners in Post Doctoral Research 2015/16 (S-HKU701/15), HKU Seed Fund for Basic Research (No. 201611159029), the Biotechnology and Biological Sciences Research Council (UK; grant BB/M029611/1), the Wellcome Trust (equipment grant WT087658), and the Scottish Life Science Alliance. The authors declare no potential conflicts of interest with respect to the authorship and/or publication of this article.

References

Attin T, Hartmann O, Hilgers RD, Hellwig E. 1995. Fluoride retention of incipient enamel lesions after treatment with a calcium fluoride varnish in vivo. Arch Oral Biol. 40(3):169–174.

Beniash E, Simmer JP, Margolis HC. 2005. The effect of recombinant mouse amelogenins on the formation and organization of hydroxyapatite crystals in vitro. J Struct Biol. 149(2):182–190.

Bruun C, Givskov H. 1993. Calcium fluoride formation in enamel from semi- or low-concentrated F agents in vitro. Caries Res. 27(2):96–99.

Chen JS, Yu ZW, Zhu PZ, Wang JF, Gan ZH, Wei J, Zhao YH, Wei SC. 2015. Effects of fluorine on the structure of fluorohydroxyapatite: a study by XRD, solid-state NMR and Raman spectroscopy. J Mater Chem B. 3(1):34–38.

Chen Y, Miao X. 2005. Thermal and chemical stability of fluorohydroxyapatite ceramics with different fluorine contents. Biomaterials. 26(11):1205–1210.

Chu CH, Lee AH, Zheng L, Mei ML, Chan GC. 2014. Arresting rampant dental caries with silver diamine fluoride in a young teenager suffering from chronic oral graft versus host disease post-bone marrow transplantation: a case report. BMC Res Notes. 7:3.

Chu CH, Lo EC. 2008. Microhardness of dentine in primary teeth after topical fluoride applications. J Dent. 36(6):387–391.

Chu CH, Lo EC, Lin HC. 2002. Effectiveness of silver diamine fluoride and sodium fluoride varnish in arresting dentin caries in Chinese pre-school children. J Dent Res. 81(11):767–770.

Chu CH, Mei L, Seneviratne CJ, Lo EC. 2012. Effects of silver diamine fluoride on dentine carious lesions induced by *Streptococcus mutans* and *Actinomyces naeslundii* biofilms. Int J Paediatr Dent. 22(1):2–10.

Eanes ED, Hailer AW. 1998. The effect of fluoride on the size and morphology of apatite crystals grown from physiologic solutions. Calcif Tissue Int. 63(3):250–257.

Gao SS, Zhao IS, Niraishi N, Duangthip D, Mei ML, Lo EC, Chu CH. 2016. Clinical trials of silver diamine fluoride in arresting caries among children a systematic review. JDR Clin Trans Res. 1(3):201–210.

Habraken WJ, Tao J, Brylka LJ, Friedrich H, Bertinetti L, Schenk AS, Verch A, Dmitrovic V, Bomans PH, Frederik PM, et al. 2013. Ion-association complexes unite classical and non-classical theories for the biomimetic nucleation of calcium phosphate. Nat Commun. 4:1507.

Kokubo T, Kim HM, Kawashita M. 2003. Novel bioactive materials with different mechanical properties. Biomaterials. 24(13):2161–2175.

Lagerlöf F, Dawes C. 1984. The volume of saliva in the mouth before and after swallowing. J Dent Res. 63(5):618–621.

Liu Y, Hsu CY, Teo CM, Teoh SH. 2013. Potential mechanism for the laser-fluoride effect on enamel demineralization. J Dent Res. 92(1):71–75.

Lou YL, Botelho MG, Darvell BW. 2011. Reaction of silver diamine [corrected] fluoride with hydroxyapatite and protein. J Dent. 39(9):612–618.

Majewski PJ, Allidi G. 2006. Synthesis of hydroxyapatite on titanium coated with organic self-assembled monolayers. Mater Sci Eng A. 420(1–2):13–20.

Mei ML, Chu CH, Low KH, Che CM, Lo EC. 2013. Caries arresting effect of silver diamine fluoride on dentine carious lesion with *S. mutans* and *L. acidophilus* dual-species cariogenic biofilm. Med Oral Patol Oral Cir Bucal. 18(6):e824–e831.

Mei ML, Ito L, Cao Y, Li QL, Chu CH, Lo EC. 2014. The inhibitory effects of silver diamine fluorides on cysteine cathepsins. J Dent. 42(3):329–335.

Mei ML, Ito L, Cao Y, Li QL, Lo EC, Chu CH. 2013. Inhibitory effect of silver diamine fluoride on dentine demineralisation and collagen degradation. J Dent. 41(9):809–817.

Mei ML, Ito L, Cao Y, Lo EC, Li QL, Chu CH. 2014. An ex vivo study of arrested primary teeth caries with silver diamine fluoride therapy. J Dent. 42(4):395–402.

Mei ML, Li QL, Chu CH, Lo EC, Samaranayake LP. 2013. Antibacterial effects of silver diamine fluoride on multi-species cariogenic biofilm on caries. Ann Clin Microbiol Antimicrob. 12:4.

Mei ML, Li QL, Chu CH, Yiu CK, Lo EC. 2012. The inhibitory effects of silver diamine fluoride at different concentrations on matrix metalloproteinases. Dent Mater. 28(8):903–908.

Ogard B, Seppä L, Rølla G. 1994. Professional topical fluoride applications—clinical efficacy and mechanism of action. Adv Dent Res. 8(2):190–201.

Peters MC, Bresciani E, Barata TJ, Fagundes TC, Navarro RL, Navarro MF, Dickens SH. 2010. In vivo dentin remineralization by calcium-phosphate cement. J Dent Res. 89(3):286–291.

Robinson C, Connell S, Kirkham J, Brookes SJ, Shore RC, Smith AM. 2004. The effect of fluoride on the developing tooth. Caries Res. 38(3):268–276.

Schwartz SS, Hay DI, Schluckebier SK. 1992. Inhibition of calcium phosphate precipitation by human salivary statherin: structure-activity relationships. Calcif Tissue Int. 50(6):511–517.

Suzuki T, Nishida M, Sobue S, Moriwaki Y. 1974. Effects of diammine silver fluoride on tooth enamel. J Osaka Univ Dent Sch. 14:61–72.

Tan HP, Lo EC, Dyson JE, Luo Y, Corbet EF. 2010. A randomized trial on root caries prevention in elders. J Dent Res. 89(10):1086–1090.

ten Cate JM. 1997. Review on fluoride, with special emphasis on calcium fluoride mechanisms in caries prevention. Eur J Oral Sci. 105(5 Pt 2):461-465.

Termine JD, Posner AS. 1970. Calcium phosphate formation in vitro: I. Factors affecting initial phase separation. Arch Biochem Biophys. 140(2):307–317.

Wei M, Evans JH, Bostrom T, Grondahl L. 2003. Synthesis and characterization of hydroxyapatite, fluoride-substituted hydroxyapatite and fluorapatite. J Mater Sci Mater Med. 14(4):311–320.

Yamaga R, Nishino M, Yoshida S, Yokomizo I. 1972. Diammine silver fluoride and its clinical application. J Osaka Univ Dent Sch. 12:1–20.